

HEAVY FLAVOR PHYSICS AT THE TEVATRON

Giorgio Apollinari

Fermi National Accelerator Laboratory

Batavia, IL 60510

Representing the D ϕ and CDF Collaborations

ABSTRACT

We report on the status of top and b quark physics at the Fermilab Tevatron collider. In particular, we summarize the knowledge obtained by CDF and D ϕ on the top quark mass and production cross section. We also present some new interesting results obtained by CDF with the discovery of the B_c meson, and a first low-statistics measurement of $\sin(2\beta)$ at a hadronic collider.

© 1998 by Giorgio Apollinari.

1 Introduction

In this paper, we present a review of recent results obtained on the subject of heavy flavor physics at the Tevatron $p\bar{p}$ collider at Fermilab. After a brief historical overview in Sec. 2, we summarize the status of top quark physics at CDF and $D\bar{D}$ in Sec. 3. In particular, we discuss the measurement of the top production cross section and the world-average direct determination of the top quark mass. Section 4 is devoted to recent B physics results at the Tevatron collider, with emphasis on a preliminary, low-statistics measurement of the time-dependent asymmetry in the decay $B^0, \bar{B}^0 \rightarrow J/\psi K_s^0$. We will also discuss the observation of the B_c meson. Finally, a brief outlook at the future prospects for top quark physics, as well as CP-violation measurements in the b sector, is given in Sec. 5.

2 Historical Overview

Heavy flavor physics at the Tevatron collider is synonymous with physics of the third quark generation. Since the discovery of the τ lepton¹ in 1976, the third quark generation has been the “most anticipated” quark family. At least part of the anticipation was based on theoretical arguments² that explained the observed CP violation in the $K^0-\bar{K}^0$ system³ through the existence of three quark families, and an appropriate mixing between the mass and the weak interaction eigenstates.

In 1977, the b quark was discovered as a dimuon resonance in 400 GeV proton-nucleus collisions at Fermilab,⁴ and soon after its discovery, the DORIS e^+e^- storage ring at DESY⁵ confirmed the existence of the Υ resonances at a mass of about 9.5 GeV/c². These narrow resonances allowed the assignment of a charge -1/3 to the newly discovered b quark.

The Standard Model (SM) is an anomaly free theory⁶ if and only if the sum of all the left-handed fermion charges in a given family is null ($\sum_l Q^l + N_c \sum_q Q^q = 0$, where N_c is the number of colored quarks, Q^l are the lepton charges, and Q^q are the quark charges in a family). Therefore, the -1/3 charge for the b quark and the existence of the τ lepton implied the existence of a b quark partner with a charge of +2/3. This partner is by definition the top quark.

Similarly, in the SM, the b and top quark are members of a weak isospin doublet, and further evidence for the existence of the top quark was produced by the weak isospin measurement of the b quark, extracted from the forward-backward asymmetry A_{FB} in

$e^+e^- \rightarrow b\bar{b}$ at PETRA⁷ and LEP-SLD,⁸ where the measurements supported the assignment of $I_3 = -1/2$ for the weak isospin of the b quark, and therefore, the necessity of a $I_3 = +1/2$ partner of the b quark.

The discovery of the top quark has been one of the goals of the Fermilab Tevatron Collider since its commissioning in 1985. However, the top quark has not been the only heavy quark studied at the Tevatron. As will be shown in Sec. 4, the Tevatron collider, and CDF in particular, have also made major contributions to the study of the b sector of the SM.

2.1 Experimental Tools

The Fermilab $p\bar{p}$ Tevatron Collider, with a center-of-mass energy of 1.8 TeV, is the highest energy collider in the world.

Designed for a peak luminosity of 10^{30} cm⁻²s⁻¹, it routinely reached luminosities of 2×10^{31} cm⁻²s⁻¹ during the 1992-1993 and 1994-1995 data-taking periods, thanks to a set of electrostatic insertions⁹ separating the beams, except at the CDF and $D\bar{D}$ intersection regions. These insertions improved the beam lifetime and decreased the beam emittance. The bunches cross every 3.5 μ s producing a luminous region with a Gaussian distribution having a width of $\sigma_x = 30$ cm along the beam line, and ~ 36 μ m in the direction perpendicular to the beams.

The CDF detector has been extensively described in detail elsewhere.¹⁰ Briefly, it consists of a magnetic spectrometer surrounded by calorimeters and muon chambers. A new low-noise, radiation hard four layer silicon vertex detector (SVX),¹¹ located just immediately outside the beam pipe, provides precise track reconstruction in the direction perpendicular to the beams ($\sigma_{d_0} \sim 17$ μ m) and is used to identify secondary vertices from b and c quark decays. The momentum of charged particles is measured in the central tracking chamber (CTC) which is immersed in a 1.4-T superconducting solenoidal magnet, with an excellent momentum resolution ($\sigma(P_t)/P_t = 0.1\%P_t \oplus 0.6\%$). Outside the solenoid, electromagnetic ($\sigma(E_{em})/E_{em} \sim 17\%/\sqrt{E_{em}}$) and hadronic ($\sigma(E_{had})/E_{had} \sim 50\%/\sqrt{E_{had}}$) calorimeters cover the whole azimuthal angle and extend to pseudorapidities of $|\eta| \sim 4.2$. They are used to identify and measure jets and electron candidates. The calorimeters are also used to measure the missing transverse energy (\cancel{E}_T) which can indicate the presence of undetected energetic neutrinos. Outside the calorimeter, drift chambers in the region $|\eta| < 1.0$ provide muon identification. A three level trigger selects inclusive electrons and muons used for the

top search. The detection efficiency for $t\bar{t}$ events is improved by the inclusion of triggers based on \cancel{E}_T .

A schematic view of the CDF detector is shown in Fig. 1(a).

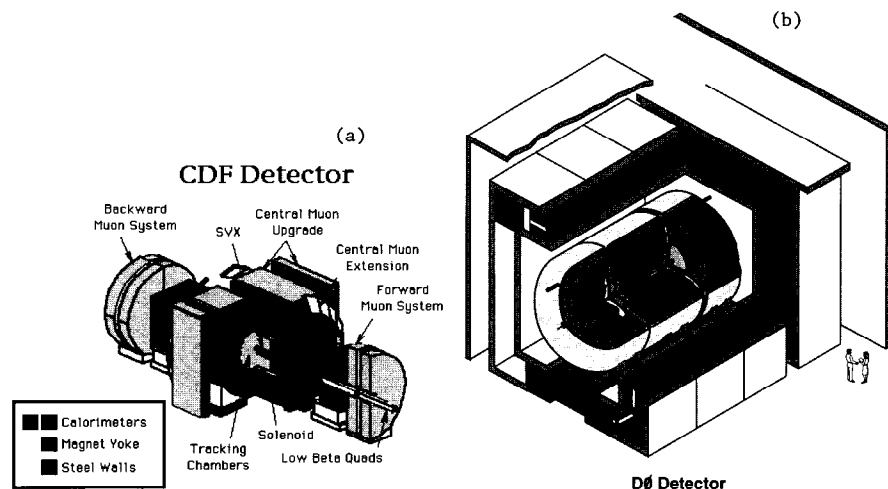


Figure 1: Isometric views of (a) CDF and (b) $D\phi$ detectors.

The $D\phi$ detector and data collection system are also described elsewhere.¹² The $D\phi$ detector has a hermetic, compensating sampling calorimeter with fine longitudinal and transverse segmentation in pseudorapidity and azimuthal angle. The energy resolutions are slightly better than those measured at CDF ($\sigma(E_{em})/E_{em} \sim 15\%/\sqrt{E_{em}}$) and ($\sigma(E_{had})/E_{had} \sim 50\%/\sqrt{E_{had}}$). Since there is no central field, charged particle tracks are reconstructed with a sign degeneracy using drift chambers located between the interaction region and the calorimeter. Electrons are identified by a transition radiation detector. Muons are detected by reconstructing tracks in proportional drift tubes before and behind a set of magnetized iron toroids located outside the calorimeter which provide some momentum measurement with a resolution of $\sigma(P_t)/P_t = 0.3\%P_t \oplus 17\%$ for pseudorapidities in the range $|\eta| < 3.0$. The good calorimeter hermeticity provides a good missing transverse energy resolution. The CDF transverse energy resolution is approximately 20% worse than $D\phi$. A schematic view of the $D\phi$ detector is shown in Fig. 1(b).

3 Top Quark at the Tevatron Collider

As mentioned previously, the top quark has been searched since the discovery of its partner, the b quark, in 1977. The first indication that the top quark was a heavy object came from the measurement of a large mixing parameter x_d in the $B^0-\bar{B}^0$ mixing, first observed by the UA1¹³ and ARGUS¹⁴ Collaborations.

Precise electroweak fits from LEP have constrained the top quark mass with ever increasing precision since the turn-on of LEP in 1990, as shown in Fig. 2.

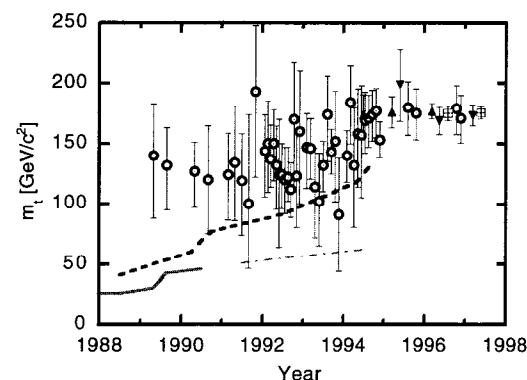


Figure 2: Historical evolution¹⁵ of the indirect fits to the top quark mass from precise electroweak measurements at LEP (circles). The solid and dashed lines indicate the 95% C.L. on the lower M_{top} bound from direct e^+e^- and $p\bar{p}$ searches. The last points are the direct measurements from CDF (triangles) and $D\phi$ (inverted triangles).

The first evidence for the top quark's existence was published by CDF¹⁶ in 1994, with a 2.8σ excess of events over the background expectations. Under the assumption of top production, CDF measured a top mass of $M_{top} = 174 \pm 16 \text{ GeV}/c^2$ and a production cross section $\sigma_{t\bar{t}} = 13.9^{+6.1}_{-4.8} \text{ pb}$. Both CDF¹⁷ and $D\phi$ ¹⁸ announced the definitive top discovery in 1995, reporting mass values of:

$$\begin{aligned} M_{top} &= 176 \pm 8 \pm 10 \text{ GeV}/c^2 \quad (\text{CDF}), \\ M_{top} &= 199^{+19}_{-21} \pm 22 \text{ GeV}/c^2 \quad (D\phi), \end{aligned}$$

and production cross sections of:

$$\begin{aligned}\sigma_{t\bar{t}} &= 6.8^{+3.6}_{-2.4} pb \quad (\text{CDF}), \\ \sigma_{t\bar{t}} &= 6.4 \pm 2.2 pb \quad (D\phi).\end{aligned}$$

At $M_{top} \sim 175 \text{ GeV}/c^2$, the top is the heaviest known elementary particle. The large mass, similar in order of magnitude to the scale for electroweak symmetry breaking, implies a Yukawa coupling for top of the order of 1, while the same coupling for the electron is a million times smaller. Is this telling us that the top quark is the only “normal” fermion, while all the other fermions “lost” part of their mass in some symmetry breaking mechanism?

On the other hand, Fig. 3 shows the rather simple mass pattern of the presently known quarks and leptons. It has been noted¹⁹ that on the logarithmic scale of Fig. 3, the large top mass is not that exceptional and seems to follow an established pattern.

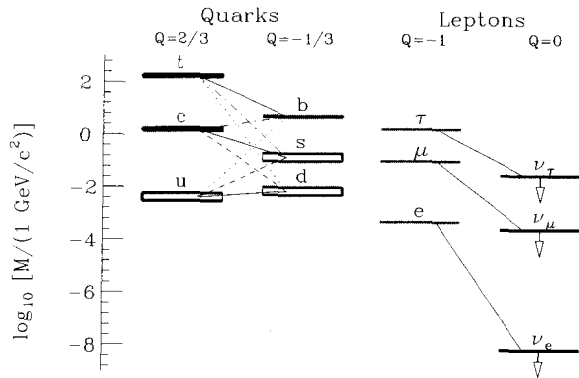


Figure 3: Quark and Lepton mass patterns¹⁹ on a logarithmic scale. The upper-bound on neutrino masses are indicated by the arrow, while the solid and dotted lines correspond to the allowed interquark and interlepton transitions.

In any case, it is clear that due to its large mass the top couples very strongly to the Higgs field, and that the lifetime of the top quark ($\tau_{top} \propto 1/(|V_{tb}|^2 \times M^3) \sim 10^{-24} \text{ sec}$) is much shorter than the typical timescale for QCD hadronization ($\tau_{QCD} \propto 1/\Lambda_{QCD} \sim 10^{-23} \text{ sec}$). This implies that the top is the only quark that can be studied in a free state, since it decays before hadronizing. Consequently, predictions from perturbative QCD

on its production rate are expected to be rather accurate. The fact that the top quark may also imply that the physics in the richness of phenomena observed in the b sector. A top quark to be created mostly from $q\bar{q}$ rather than gg interact to $\sim 90\%$ of the total $\sigma_{t\bar{t}}$. The NLO calculations²⁰ where the NLO corrections contribute approximately 10% to the total cross section, and the contributions of initial and final state radiation are

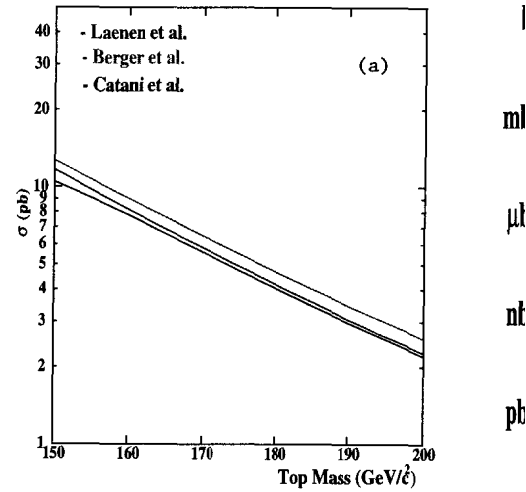


Figure 4: NLO calculation for (a) $\sigma_{t\bar{t}}$ as a function of top mass. The curves represent different production processes.

Figure 4(b) gives a simple pictorial view of the phenomena at the Tevatron Collider. As can be seen, the production is expected to be ~ 3 times lower than $\sigma_{t\bar{t}}$, which is the subject of study for CDF and D ϕ .

In the SM, assuming V-A coupling and $|V_{ti}| \sim 1$, the top quark decays through the channel $t \rightarrow Wb$. The decays $t \rightarrow Wc$ are suppressed by factors of $|V_{ts}|^2/|V_{tb}|^2 \sim 10^{-3}$ and $|V_{tc}|^2/|V_{tb}|^2 \sim 10^{-3}$. The signature of $t\bar{t}$ events is characterized by the presence of the decay modes of the two W's present in the event, following three channels:

- Dilepton channel (ee , $\mu\mu$, or $e\mu$), corresponding to a branching ratio of $\sim 5\%$ of the total decay.
- Lepton + jets channel (e or μ), corresponding to a branching ratio of $\sim 30\%$.
- Hadronic channel, corresponding to the remaining $\sim 45\%$ of the total decay.

In addition, there are $\sim 21\%$ of the $t\bar{t}$ decays containing a τ lepton in the final state.

3.1 Top Quark Production at the Tevatron Collider

3.1.1 Dilepton Channel

Given the process $t\bar{t} \rightarrow W^+W^-b\bar{b} \rightarrow l^+l^-\nu\bar{\nu}b\bar{b}$, the final state for this channel is determined by two oppositely charged leptons with high transverse momenta, large \cancel{E}_T , and two b -jets. The dominant backgrounds are WW , $Z \rightarrow \tau^+\tau^-$, and the Drell-Yan production. The dilepton channel is expected to have a very good signal-to-background ratio. However, this decay mode is still limited by statistics, and therefore, not ideal (yet) for a precise measurement of the top mass.

The CDF *dilepton* search starts with the identification of a lepton (e or μ) with $P_T > 20$ GeV/ c and satisfying a set of isolation requirements in the central region ($|\eta| < 1.0$). The second lepton is required to have $P_T > 20$ GeV/ c and to satisfy a looser set of isolation requirements. The two leptons must be oppositely charged, and events with ee or $\mu\mu$ candidates where the invariant mass is between 75 and 105 GeV/ c^2 are rejected as being consistent with Z^0 candidates.

In order to reject the Drell-Yan events, CDF requires $\cancel{E}_T > 25$ GeV. For events with $\cancel{E}_T < 50$ GeV, the azimuthal angle between the \cancel{E}_T and the closest lepton or jet must be greater than 20° to reduce the background coming from $Z \rightarrow \tau\tau$ and Drell-Yan events, where a mismeasured jet produces an artificial \cancel{E}_T . Finally, all the events are required to have at least two jets with $E_T^{jet} > 10$ GeV and $|\eta| < 2.0$. Background contributions are estimated from a combinations of data and Monte Carlo simulations.

Figure 5(a) shows the distribution of the nine dilepton candidates (one ee , one $\mu\mu$, and seven $e\mu$ events) surviving these cuts in the total integrated luminosity of $110 pb^{-1}$ at CDF.

The $D\phi$ analysis proceeds in a parallel way, the major differences being the cuts on the lepton P_T ($P_T > 15$ (20) GeV/ c for the $e\mu, \mu\mu$ (ee) channels) and a minimum requirement on H_T ($H_T > 120$ GeV for the “electron” channels, or $H_T > 100$ GeV for the “muon” channel). H_T is defined as the scalar sum of the transverse energies E_T^{jet} of

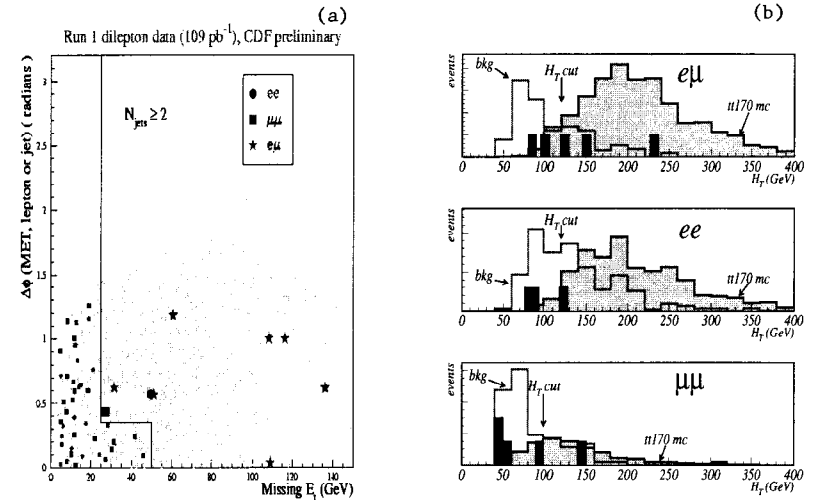


Figure 5: The azimuthal angle $\Delta\phi$ between the \cancel{E}_T vector and the nearest lepton or jet vs \cancel{E}_T in CDF dilepton events. (a) The small points show the distribution expected for the $t\bar{t}$ signal, while the larger symbols represent the data. (b) H_T distributions of dilepton events in the $D\phi$ analysis. The observed events are shown by the darker histograms.

Table 1: Summary of the *dilepton* counting experiments.

Sample		D ϕ	CDF
$e\mu$	Observed	3	7
	Background	0.3 ± 0.1	0.8 ± 0.2
	Expected ($M_{top} \approx 175 \text{ GeV}/c^2$)	1.7 ± 0.3	2.5 ± 0.2
ee or $\mu\mu$	Observed	2	2
	Background	1.1 ± 0.4	1.6 ± 0.5
	Expected ($M_{top} \approx 175 \text{ GeV}/c^2$)	1.4 ± 0.1	1.6 ± 0.2
$e\tau$ or $\mu\tau$	Observed	—	4
	Background	—	1.96 ± 0.35
	Expected ($M_{top} \approx 175 \text{ GeV}/c^2$)	—	0.7 ± 0.1

the jets (for the $\mu\mu$ channels) or the scalar sum of the E_T 's of the leading e and the jets (for the $e\mu + jets$ and $ee + jets$ channels). Figure 5(b) shows the discriminating power of the H_T variable for $M_{top} = 200 \text{ GeV}/c^2$ and the dilepton events surviving the D ϕ selection.

The tests performed by D ϕ to understand the behavior of H_T for background events include the comparison between data and Monte Carlo in background-dominated channels such as $e + 2$ jets and $e + 3$ jets, where the H_T distribution agrees well with background calculations based on the VECBOS Monte Carlo and multijet events. D ϕ observes three $e\mu$, one ee , and one $\mu\mu$ candidate.

In both experiments, the acceptance is much higher for the $e\mu$ than for the ee and $\mu\mu$ channels because of the cut to reject Z^0 candidates. Table 1 summarizes the *dilepton* counting experiments results.

The production cross section is determined through the standard formula:

$$\sigma_{t\bar{t}} = \frac{N - B}{\epsilon \int L dt}, \quad (1)$$

where N is the observed number of events, B is the expected background (determined from a combination of data and Monte Carlo), ϵ is the total efficiency, and $\int L dt$ is the integrated luminosity. The efficiency depends on the mass of the top quark, and the two experiments determined the efficiencies for the top quark mass corresponding to the respective direct mass measurement ($\sim 175 \text{ GeV}/c^2$ for CDF and $\sim 172 \text{ GeV}/c^2$ for

D ϕ). The values determined by the two experiments are:

$$\sigma_{t\bar{t}} = 8.2^{+4.4}_{-3.4} \text{ pb} \quad (\text{CDF})$$

$$\sigma_{t\bar{t}} = 5.0 \pm 3.3 \text{ pb} \quad (\text{D}\phi)$$

3.1.2 $e\nu$ Channel

A top quark decay channel recently explored by D ϕ is the $t \rightarrow e\nu$ channel, based on the requirement of one isolated electron \cancel{E}_T and one neutrino \cancel{E}_T with transverse momentum greater than 20 GeV. A cut on the scalar sum of the mass of the electron and \cancel{E}_T is designed to reject the Z^0 background. The $M_T(e\nu) > 150 \text{ GeV}/c^2$. This inclusive selection, with the subdivision of the events into *dilepton* and *electron + neutrino* channels, increases the top acceptance. With the selection cuts, the sample is expected to contain 50% dilepton decays, 33% $e\nu$ decays, and 17% of $e\tau$ decays. Figure 6 shows the data distribution and Monte Carlo data distributions for comparison. D ϕ finds four events, and measures²⁴ a cross section of

$$\sigma_{t\bar{t}} = 9.6 \pm 7.5 \text{ pb} \quad (\text{D}\phi)$$

When combined with the previous dilepton measurement, the cross section is

$$\sigma_{t\bar{t}} = 6.4 \pm 4.4 \text{ pb} \quad (\text{D}\phi \text{ dilepton})$$

3.1.3 *Lepton + Jets* Channel

Given the process $t\bar{t} \rightarrow W^+W^-b\bar{b} \rightarrow l\nu q\bar{q}l$, the l is a lepton with high transverse momentum, large \cancel{E}_T , two jets, and two b -jets. The set of cuts used in the top quark search to define the signal region of $W + \geq 3$ jets, the cuts used to reject the expected $t\bar{t}$ signal (70% in the case of a $175 \text{ GeV}/c^2$ top quark) and the QCD $W +$ multijet background.

However, after the removal of Z^0 candidates, the level of 1/6 (for example, CDF is left with ~ 30 events). The background contributions are coming from $W +$ multijet production (~ 160 expected events) with small contributions from $t\bar{t}$ production.

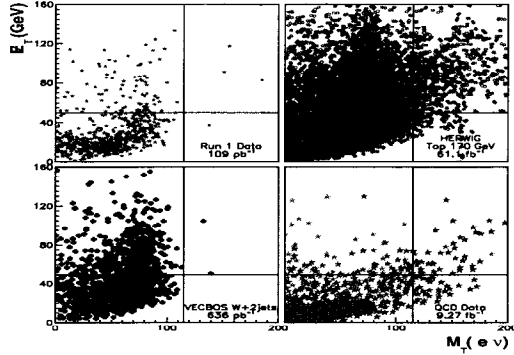


Figure 6: Aplanarity vs H_T for the $e\nu$ analysis in $D\phi$ for data, $t\bar{t}$ Monte Carlo events, multijet background, and $W + 4$ jets Monte Carlo background. The dashed lines indicate the cuts.

$b\bar{b}$ jets (~ 30 events), $Z \rightarrow ll$ (~ 26 events), and diboson production (~ 15 events). Clearly, additional background rejection is required. $D\phi$ and CDF solve the problem of the rejection of W +jets QCD backgrounds with three different approaches:

- Event Shape analysis²⁴ ($D\phi$). This approach relies on the fact that, for heavy top, the overall event is different (more *spherical*, and with more energy) than normal QCD $W +$ multijet events. The variables used by $D\phi$ to discriminate against background include the event aplanarity \mathcal{A} and the already-mentioned H_T . No attempt is made at the identification of the original flavor of the jets in the event.
- b -quark tagging through the semileptonic decay (CDF²⁵ and $D\phi$ ²⁴). This approach identifies the b -nature of the jets present in the event through the presence of a soft lepton embedded in the jets and originated by a semileptonic decay of the parent b quark (SLT, or Soft Lepton Tagging).
- b -quark tagging by mean of displaced vertices or displaced tracks (CDF²⁵). This approach relies on the finite b -quark lifetime and the superb precision of the Silicon Vertex (SVX) detector to identify displaced vertices (SECVTX tagging) or displaced tracks (JPB tagging).

Table 2: Cuts used by CDF and $D\phi$ for the $lepton + jets$ search.

	CDF	$D\phi$	
	All	$e(\mu)$	$e + jets/\mu$
P_T^l	20 GeV	20 GeV	20 GeV
\cancel{E}_T	20 GeV	25(20) GeV	20 GeV
Number of Jets	$\geq 3, \eta < 2$	$\geq 4, \eta < 2.5$	$\geq 4, \eta < 2.5$
E_T^{jet}	≥ 15 GeV	≥ 15 GeV	≥ 20 GeV
\mathcal{A}	-	> 0.065	> 0.040
H_T	-	> 180 GeV	> 110 GeV

The typical efficiencies per b -quark jet for the three tagging tools are $\sim 23\%$ (SECVTX), $\sim 22\%$ (JPB), and $\sim 7\%$ (SLT). Clearly, due to the different lifetime and decay kinematics, the efficiencies of these tagging tools for c -quark jets are different [$\sim 4\%$ (SECVTX), $\sim 9\%$ (JPB), and $\sim 4\%$ (SLT), respectively] and can be used to select samples of data with different c -quark and b -quark compositions.

Figure 7 shows the number of observed W + multijet events after the SVX and SLT tagging algorithms in CDF. The background expectations are based on a mistag rate measured in inclusive jets, while the fraction of W + multijet events due to $Wb\bar{b}$, $Wc\bar{c}$, or Wc are estimated from the Monte Carlo using the measured tagging efficiency. In the $W + 1 \text{ jet}$ bin, which is expected to be completely populated by background, the observed data are in good agreement with expectations.

The excess of events in the $W + 3$ - and $W + 4$ -jet bins are attributed completely to top production.

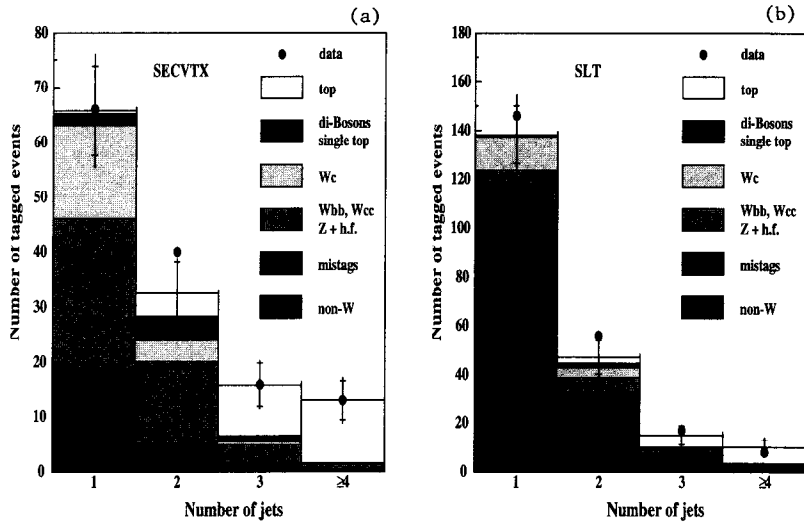


Figure 7: The CDF jet multiplicity distribution of (a) SVX tagged and (b) SLT tagged lepton + jets events.

Figure 8 shows the $D\phi$ distribution of events in \mathcal{A} and H_T variables for the data and various Monte Carlo simulations.

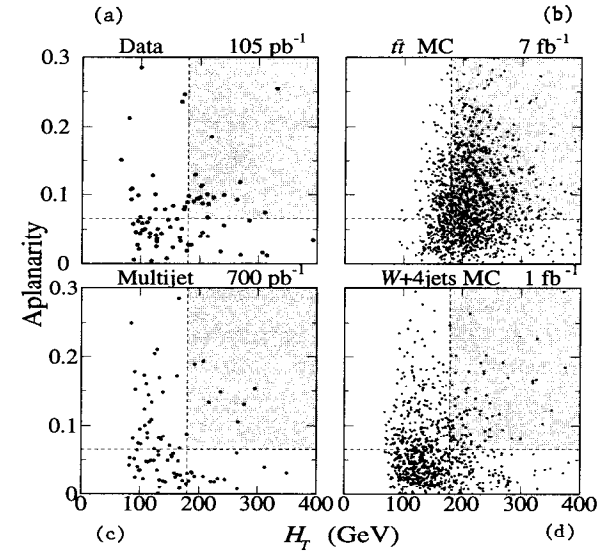


Figure 8: Aplanarity vs H_T for the $D\phi$ lepton + jets events for (a) data, (b) $t\bar{t}$ Monte Carlo, (c) multijet background, and (d) W + jets VECBOS Monte Carlo.

Table 3 gives the total number of observed events and the expected background and signals for the two experiments. The cross sections measured by CDF and $D\phi$ are:^{24,25}

$$\begin{aligned}\sigma_{\bar{t}\bar{t}} &= 6.2^{+2.1}_{-1.7} \text{ pb} & (\text{CDF} - \text{SVX}) \\ \sigma_{\bar{t}\bar{t}} &= 9.2^{+4.3}_{-3.6} \text{ pb} & (\text{CDF} - \text{SLT}) \\ \sigma_{\bar{t}\bar{t}} &= 4.1 \pm 2.1 \text{ pb} & (D\phi - \text{Event Shape}) \\ \sigma_{\bar{t}\bar{t}} &= 8.3 \pm 3.5 \text{ pb} & (D\phi - \text{SLT}).\end{aligned}$$

3.1.4 Hadronic Top Search

The final state for the full hadronic decay of the top consists of six jets, two of them being b -quark jets. The event selection in CDF starts with the requirement of ≥ 5 jets with $E_T > 15 \text{ GeV}$ and $|\eta| < 2.0$. The background, coming predominantly from QCD multi-jet events, is large even after tagging of the b -quarks as shown from the Monte Carlo predictions in Table 4.

In order to further reduce the background, CDF applies a kinematical selection²⁶

Table 3: Summary of the *lepton + jets* counting experiments.

Sample		$D\phi$	CDF
Event Shape	Observed	19	22
	Background	9.7 ± 1.7	7.2 ± 2.1
	Expected ($M_{top} \sim 170$ GeV)	14.1 ± 3.1	—
$b \rightarrow lX$	Observed	11	40
	Background	2.4 ± 0.5	24.3 ± 3.5
	Expected ($M_{top} \sim 170$ GeV)	5.8 ± 1.0	9.6
Displaced Vertex	Observed	—	34 Events (42 Tags)
	Background	—	8.4 ± 1.4
	Expected ($M_{top} \sim 170$ GeV)	—	19.8 ± 4.0

Table 4: Predicted signal and backgrounds in the CDF Hadronic Top search.

$\frac{S}{S+B}$	≥ 5 jets	≥ 6 jets
No tag	1/500	1/200
1 b - tag	1/100	1/30
2 b - tag	1/20	1/10

which includes requiring the $\Sigma E_T \geq 300$ GeV and $C > 0.75$, where the centrality C is defined as $C = H_T/\sqrt{\hat{s}}$ and \hat{s} is the invariant mass of the multijet system. After these kinematical cuts a requirement of one b -tagged jet produces the multiplicity distribution shown in Fig. 9(a) which shows a clear excess of events over the expected background from QCD contributions.

A similar analysis from $D\phi$ ²⁷ uses a selection based on the discriminating power of a neural network fed with 14 variables which include kinematical quantities (like aplanarity and total scalar energy) as well as soft lepton tagging of b -quark jets. The output of the neural network is shown in Fig. 9(b).

The cross section values obtained by the two collaborations for the all-hadronic decay modes are:

$$\begin{aligned}\sigma_{t\bar{t}} &= 10.1^{+4.5}_{-3.6} \text{ pb} \quad (\text{CDF}) \\ \sigma_{t\bar{t}} &= 7.1 \pm 3.2 \text{ pb} \quad (D\phi).\end{aligned}$$

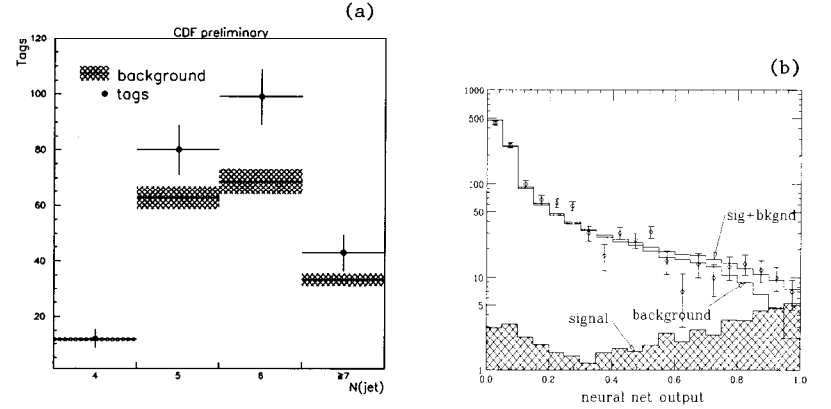


Figure 9: (a) CDF multiplicity distribution for *all hadronic* analysis with the tagged events and the background expectation. (b) Distribution of the final neural network output in the $D\phi$ *all hadronic* analysis, showing the results of a fit of the observed tagged distribution to the predictions for signal and background, with $M_{top} = 180$ GeV/ c^2 .

3.1.5 Summary of the $\sigma_{t\bar{t}}$ Cross-Section Measurements

The summary of the $\sigma_{t\bar{t}}$ cross-section measurements performed at the Tevatron is shown in Fig. 10. The $D\phi$ and CDF measurements are in good agreement with the average²⁸ of $\sigma_{t\bar{t}} = 6.7 \pm 1.3$ pb, which is slightly larger than, but still in good agreement with, the theoretical SM predictions of Fig. 4.

3.2 Top Mass Determination

A precise measurement of the top quark mass plays a central role in our understanding of the mechanism for the symmetry breaking in the SM. A precise direct measurement can provide a consistency check of the experimental data from different sources, and a combination of the top and W mass measurements provides information on the mass of the Higgs boson.

As for the cross-section measurement, the top mass determination can be performed in any one of the three different decay topologies of the $t\bar{t}$ event (*dilepton*, *lepton + jets*, and *all hadronic*). At the time of the top discovery, the *lepton + jets* channels were studied more extensively given the relative large signal-to-background ratio,

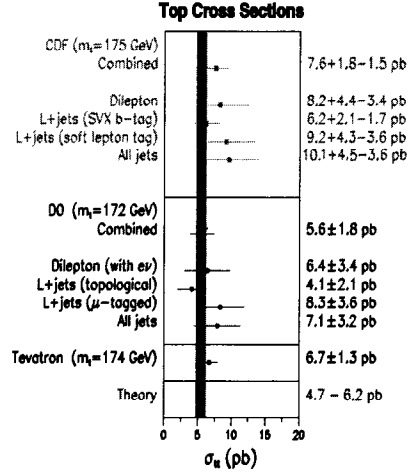


Figure 10: The $t\bar{t}$ production cross section measured in the channels studied by CDF and $D\phi$. Also shown is the range of theoretical predictions.

the large branching ratio, and the possibility of performing a constrained fit to the top mass hypothesis. As a result, in 1995 the top mass was known with an uncertainty of ~ 20 GeV/ c^2 . Since then both collaborations improved their understanding of systematic errors and the analysis of the *dilepton* and *all hadronic* decay channels, developing tools which are allowing the knowledge of the top quark mass with a very good precision (~ 5 GeV/ c^2 i.e., $\sim 3\%$). The following sections will describe the top mass measurements by $D\phi$ and CDF, as well as the average mass determined by the two experiments.

3.2.1 Lepton + Jets Channel

The hypothesis under study includes:

- $p\bar{p} \rightarrow t_1\bar{t}_2 + \text{anything}$,
- $t_1 \rightarrow Wb \rightarrow l\nu j_1$, and
- $t_2 \rightarrow Wb \rightarrow j_2 j_3 j_4$.

The use of known masses and energy-momentum conservation gives a 2C fit since there are 52 variables, 34 measured (or known) quantities, and 20 equations of conservation (the mass constraints being $M(l\nu) = M_W^{PDG}$, $M(j_2 j_3) = M_W^{PDG}$, and $M_{t_1} = M_{t_2}$).

Clearly, the method is usable only if all four jets are observed in a top decay. In CDF,²⁹ the event selection starts with the usual lepton ($P_T^l > 20$ GeV/ c) and \cancel{E}_T requirements ($\cancel{E}_T > 20$ GeV). At least four jets are required in each event, three of which must have an observed $E_T \geq 15$ GeV and $|\eta| \leq 2$. In order to increase the acceptance, the requirements on the fourth jet is relaxed to be $E_T > 8$ GeV and $|\eta| < 2.4$, provided one of four leading jets is tagged by the SVX or SLT algorithms. SVX tags are only allowed on the three leading jets ($E_T > 15$ GeV), while SLT tags are allowed on all the jets. If no such tag is present, the fourth jet must satisfy the same E_T and η requirements as the first three. The above selection defines a mass sample containing 83 events. Following the 2C fitting scheme described above, CDF requires that SVX and SLT-tagged jets are assigned to b -partons and chooses the configuration with lowest χ^2 out of the many possible combinatorial combinations. Events with $\chi^2 > 10$ are rejected. The precision of the top quark mass measurement is expected to increase with the number of observed events, the signal-to-background ratio, and the narrowness of the reconstructed-mass distribution. Monte Carlo studies demonstrated that the optimal way to partition the sample consists of subdividing the events into the four statistically independent subsamples shown in Fig. 11(a). In each distribution, the inset shows the shape of the log-likelihood function. A combination of the four different samples is shown in Fig. 11(b).

Table 5: Summary of systematic uncertainties in the CDF top mass measurements.

Source	Dilepton	Lepton + jets	All Hadronic
Jet E_T	3.8	4.4	5.0
Gluon Radiation	3.1	2.6	1.8
Background	0.3	1.3	1.7
PDF, Monte Carlo	1.1	0.5	1.0
Total	4.8	5.3	5.7

From this, CDF measures $M_{top} = 175.9 \pm 4.8$ GeV/ c^2 , where the uncertainty corresponds to a half-unit change in the negative log-likelihood with respect to its minimum.

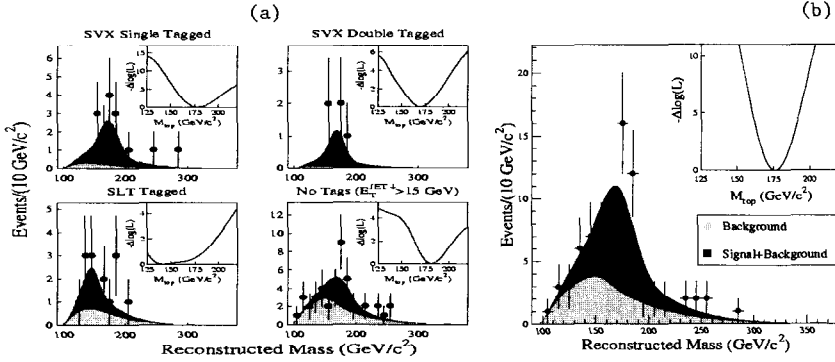


Figure 11: CDF top quark mass distributions for the $lepton + jets$ sample. The points are the data, the dark area is the top signal+background resulting from the fit, while the lightly shaded area is the background alone. The plots on (a) show the four independent samples, while (b) shows the combination of the four samples.

The CDF systematic uncertainties for the various $t\bar{t}$ decay modes considered here are listed in Table 5. The final measurement is

$$M_{top} = 175.9 \pm 4.8(stat.) \pm 4.9(syst.) \text{ GeV}/c^2 \quad (CDF - lepton + jets).$$

$D\phi$ performs a two-dimensional likelihood fit to extract the top mass value. One variable in the two-dimensional distribution is the best fit mass obtained by the 2C analysis of the data. The other variable is a top discriminant, which provides a distinct separation between the top signal and the background, without biasing the mass analysis. $D\phi$ uses two discriminants³⁰ based on the following four variable:

- \cancel{E}_T
- \mathcal{A}
- $H_{T2}/\sum|p_z|$, where H_{T2} is defined as the H_T minus the E_T of the leading jet. This variable measures the centrality of the event.
- $(\Delta R_{jj}^{min})E_T^{min}/(E_T^L + \cancel{E}_T)$, where (ΔR_{jj}^{min}) is the minimum ΔR between all pairs of jets and E_T^{min} is the smaller jet E_T from the minimum ΔR pair. This variable measures the extent to which the jets are clustered together.

These variables are combined in a Neural Network (NN) and a Low Bias (LB) discriminant to provide the kind of separation illustrated in Fig. 12(a). $D\phi$ then fits the two-dimensional distributions to templates determined from simulated $t\bar{t}$ events and background estimated using a combination of Monte Carlo and data. The experiment obtains a mass measurement of $M_{top} = 173.3 \pm 5.6(stat.) \text{ GeV}/c^2$ shown in Fig. 12(b). The systematic effects, coming mostly from the jet energy scale and the Monte Carlo modeling, sum to $\pm 5.5 \text{ GeV}/c^2$. The final mass obtained by $D\phi$ in the $lepton + jets$ channel is:

$$M_{top} = 173.3 \pm 5.6(stat.) \pm 5.5(syst.) \text{ GeV}/c^2 \quad (D\phi - lepton + jets). \quad (b)$$

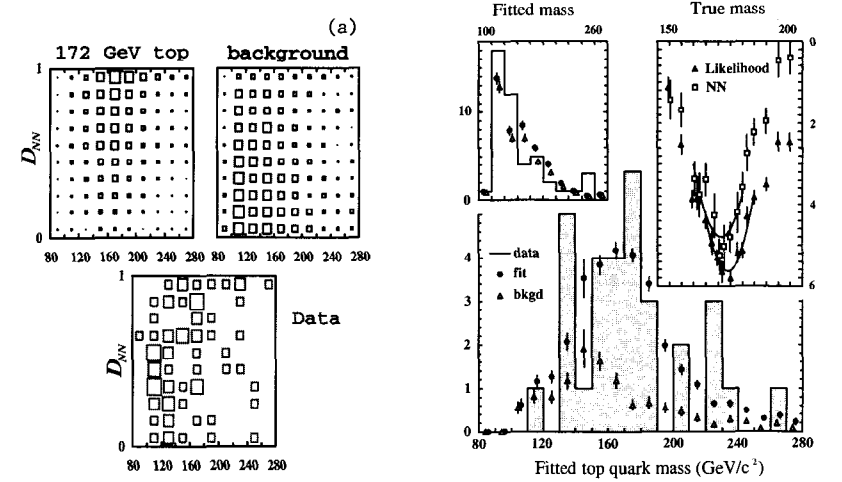


Figure 12: (a) Events per bin in the D_{NN}, m_{fit} plane for the $D\phi$ neural network discriminant analysis, showing the expectation for top, background, and data. (b) Results from the $D\phi$ $lepton + jets$ mass analysis with the D_{LB} discriminant for events poor in top signal, rich in top signal, and the final log-likelihood distribution.

3.2.2 Dilepton Top Mass Measurement

Due to the presence of two neutrinos, dilepton events do not contain enough information for a constrained fit. Therefore, to determine the top mass, one must use some other

mass estimators. One possibility is the determination of the top mass through the study of kinematic variables which have a mass dependence, like the b -jet energy spectrum ($\langle E_b \rangle \propto M_{top}$) or the invariant mass of a lepton and b -jet coming from the same top quark. These methods were originally used by CDF²³ but are limited by a rather large systematic error ($\sigma_{M_{top}} \sim 10 \text{ GeV}/c^2$).

DØ developed a method similar to the one used in the $lepton + jets$ analysis. The missing constraint in the dilepton events is provided by assuming a top quark mass and reconstructing the event for every assumed top mass.³¹ Then a weight is computed which characterizes the probability for the event to be from a $t\bar{t}$ decay with the assumed mass. DØ developed two algorithms to determine the weight. The matrix element weighting (MTW) uses the proton structure function and the probability density function for the energy of the decay lepton in the rest frame of the top quark. The neutrino weighting method (ν WT) assigns the weight based on the available phase space for the neutrinos, consistent with the measured \cancel{E}_T . A maximum likelihood fit is then performed to shape the weight distribution, using the Monte Carlo derived probability density function for signal and background, as shown in Fig. 13.

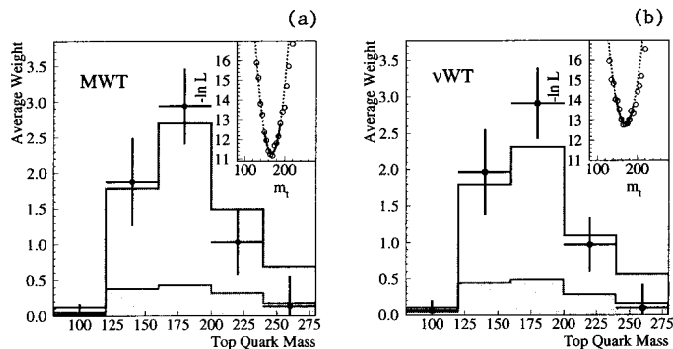


Figure 13: Sum of the normalized candidate likelihoods for (a) MWT and (b) ν WT analyses, compared to the results of the likelihood fit. The solid histogram is the best-fit $t\bar{t}$ signal plus background, and the dotted histogram is the background alone.

By using the full information of the event, the total systematic error on the measured mass is lower ($\sim 4 \text{ GeV}/c^2$) and the precision of the measurement is limited by the available statistics. DØ determined

$$M_{top} = 168.4 \pm 12.3(stat.) \pm 3.6(syst.) \text{ GeV}/c^2 \quad (D\phi - dilepton).$$

CDF applied a similar technique, assuming $atop$ quark rapidity (η) values, to solve for the neutrino momenta to each solution by comparing the sum of the neutrino solution to the measured \cancel{E}_T . For each choice of the (100) pairs of (η_1, η_2) combinations are summed to get particular mass. The mass is then varied, to generate the Fig. 14(a) for each event. From each distribution, an average is then taken, and the averages are then fit together with the Monte Carlo and top signal as shown in Fig. 14(b). Including the systematic error, the top quark mass is measured²⁹ to be:

$$M_{top} = 167.4 \pm 10.3(stat.) \pm 4.8(syst.) \text{ GeV}/c^2$$

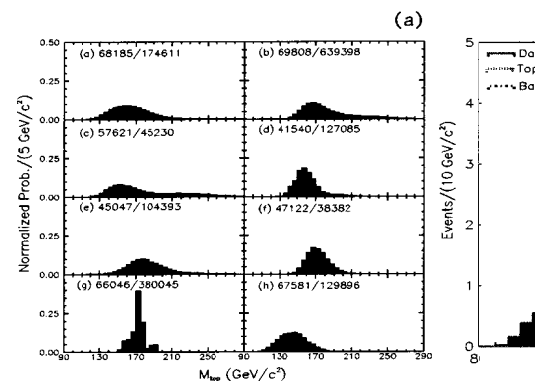


Figure 14: Weight distributions normalized to unity as eight CDF dilepton candidates, and (b) reconstructed $t\bar{t}$ events. The data are shown by the solid line, the background area and the top Monte Carlo plus the background contour.

3.2.3 Hadronic Top Mass

CDF performed a mass analysis of the $t\bar{t}$ event in which the final states are hadronic quark-antiquark pairs. The study of this channel, which complements the leptonic modes, and the mass measurement is limited by the available statistics, but it suffers from very large

reduce this background, events with at least one identified SVX b -jet are required to pass strict kinematic criteria that favor $t\bar{t}$ production and decay. To determine the top quark mass, full kinematic reconstruction is applied to the sample of events with six or more jets. All combinations are tried, with the constraint that an SVX-tagged jet must be assigned to a b -parton. The data sample consists of 136 events, of which 108 ± 9 events are expected to come from background. The reconstructed three-jet mass distribution is shown in Fig. 15. The inset shows the shape of the difference log-likelihood as a function of top mass. With the systematic uncertainty shown in Table 5, the CDF measurement²⁹ is:

$$M_{top} = 186.0 \pm 10.0(stat.) \pm 5.7(syst.) \text{ GeV}/c^2 \quad (\text{CDF} - \text{all hadronic}).$$

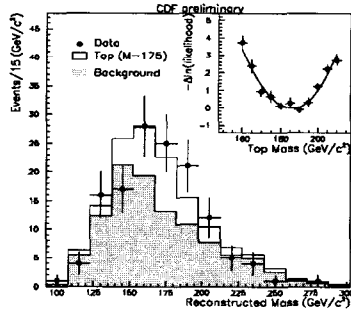


Figure 15: Reconstructed mass distribution for *all hadronic* events with at least one b -tag. Also shown are the background distribution (shaded) and the $t\bar{t}$ Monte Carlo events added to background (hollow). The inset shows the log-likelihood and the fit used to determine the top mass.

3.2.4 Top Mass Summary

Figure 16(a) shows the summary of the direct measurements of the top quark mass at the Tevatron collider. When the appropriate correlations are taken into account between the mass systematic errors in CDF and $D\phi$, the world average is determined to be

$$M_{top} = 174.3 \pm 5.1 \text{ GeV}/c^2 \quad (\text{Tevatron average}).$$

Figure 16(b) shows the relative weight of the various mass determinations on the final Tevatron average. When the top and W boson masses are interpreted in the framework of the SM, Fig. 17 shows the correlation between the top and the W masses as a function of the Higgs mass. With the latest values of the W and top masses and the LEP measurements³² the data seems to favor a light Higgs, with $m_H < 260 \text{ GeV}/c^2$ at 95% C.L.

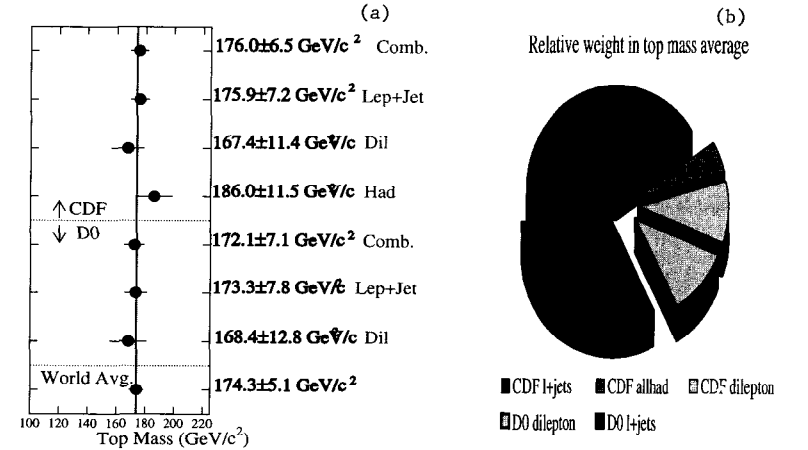


Figure 16: Summary of all the top quark mass measurements from (a) CDF and $D\phi$, and (b) relative weight of the various single measurements in the overall average.

3.3 Other Top Quark Measurements

3.3.1 Measurement of $|V_{tb}|$

In the previous discussions, $|V_{tb}|$ has been assumed to be approximately equal to 1. From the knowledge of the tagging efficiencies, the number of dilepton, and *lepton + jets* events with one, two, or no jets tagged as b quark, the following ratio can be derived:

$$R = \frac{B(t \rightarrow Wb)}{B(t \rightarrow Wq)} = \frac{|V_{tb}|^2}{|V_{tb}|^2 + |V_{td}|^2 + |V_{ts}|^2}.$$

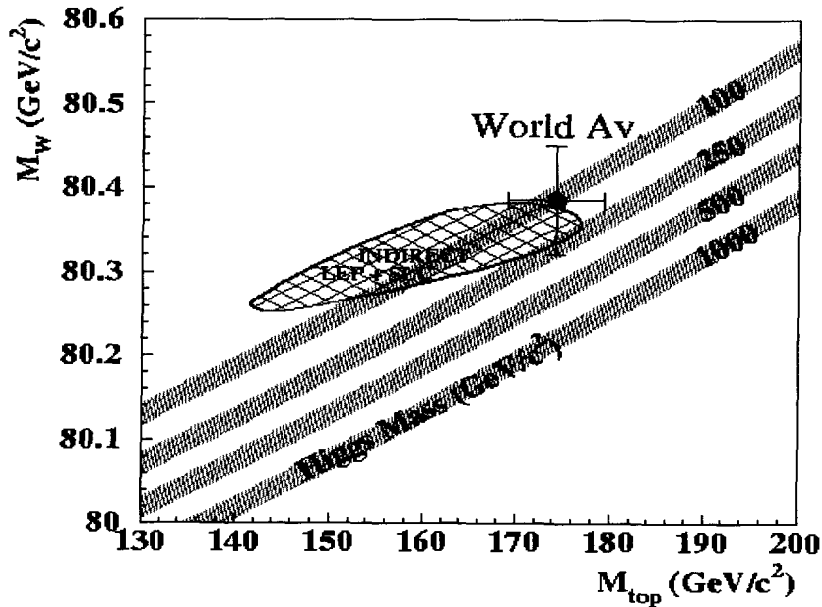


Figure 17: Relation between the top quark mass and the W boson mass. The dependence on the Higgs mass is shown through the different bands for several assumptions of m_H .

CDF has determined³³ $R = 0.99 \pm 0.29$, where the uncertainty is dominated by the statistical component. If three-generation unitarity is assumed, then $|V_{tb}| = 0.99 \pm 0.15$ and $|V_{tb}| \geq 0.76$ at 95% C.L. If the unitarity condition is relaxed, then by setting $|V_{td}| = 0.009$ and $|V_{ts}| = 0.04$ (midpoint of their 90 % C.L. determined with the unitarity assumption) CDF determines $|V_{tb}| \geq 0.048$ at 95 % C.L.

3.3.2 Flavor-Changing Neutral Current (FCNC) Decays of the Top Quark

FCNC decays can be used to probe for new physics at mass scales which are otherwise not accessible to present-day experiments. A typical historical example is the absence of the FCNC decay $K_L^0 \rightarrow \mu^+ \mu^-$ which was indicative of the existence of the charm quark, a state much heavier than the kaon.³⁴ The SM expectations for FCNC decays of the top quark are extremely small, and therefore, any observation of these modes would be evidence for physics beyond the SM.

CDF searched for $t \rightarrow q\gamma$ and $t \rightarrow qZ$. A single event is observed in the $q\gamma$ mode. Without any subtraction of the expected background, CDF finds

$$B(t \rightarrow u\gamma) + B(t \rightarrow c\gamma) < 0.032.$$

Similarly, in the $t \rightarrow qZ$ channels, with $Z \rightarrow \mu^+ \mu^-$ or $Z \rightarrow e^+ e^-$, CDF finds one candidate, and with no background subtraction the branching fraction limit is

$$B(t \rightarrow uZ) + B(t \rightarrow cZ) < 0.33.$$

This search is less sensitive than the $t \rightarrow q\gamma$ search because of the small branching fraction of the Z boson into charged leptons.

3.3.3 W Boson Helicity in Top Quark Decays

The W boson from the top decay can be polarized either transversely or longitudinally. The SM prediction for the fraction of longitudinally polarized bosons is $F_0 = M_{top}^2 / (2M_W^2 + M_{top}^2) \sim 0.70$ for $M_{top} = 174 \text{ GeV}/c^2$. A measurement of F_0 can be extracted from the P_T distribution of the observed leptons, since transversely polarized W bosons emit the charged lepton in a direction preferentially antiparallel to the direction of the boost from the top quark rest frame to the W boson rest frame, while longitudinally polarized W's emit the charged lepton perpendicular to the boost direction. Fitting simultaneously the lepton P_T spectrum in the dilepton and lepton+jets

events (Fig. 18), CDF³⁵ finds

$$F_0 = 0.55 \pm 0.32(stat.) \pm 0.12(syst.).$$

4 b Quark at the Tevatron

The principal motivation for studying b -quark physics in the context of the SM arises from the possibility of gathering valuable information on the CKM matrix elements. In fact, a study of b decays allows access to five of the nine CKM elements (V_{cb} , V_{ub} , V_{td} , V_{ts} , and V_{tb}), some of which (V_{td} , V_{ts}) would be very hard to study in decays of the top quark system.

Traditionally, b -quark physics has been the domain of e^+e^- machines. However, UA1 already demonstrated the possibility of studying b physics at a hadron collider. CDF, with a superb mass resolution and vertex detection capabilities, has really expanded the b -physics program achievable at a hadron collider. The $D\phi$ experiment has also published several b -physics results,³⁶ but due to the lack of precision momentum measurement of charged particles and the absence of a precision microvertex detector, $D\phi$ is not ideally suited to study the b sector with the same broad coverage.

A hadron machine has several advantages (and some disadvantages) compared to an e^+e^- machine at the $\Upsilon(4S)$. All species of B hadrons can be produced at the Tevatron Collider (B^+ , B^0 , B_s^0 , B_c , and Λ_b), with a large production cross section ($\sigma_b \sim 50 \mu b$, while $\sigma_{\Upsilon(4S)} \sim 1$ nb and $\sigma_{Z^0 \rightarrow b\bar{b}} \sim 7$ nb at LEP). This very large cross section results in about 5×10^9 $b\bar{b}$ pairs produced during Run I at the Tevatron detectors. Unfortunately, the inelastic cross section is three orders of magnitude larger, which puts very specific requirements on the trigger system designed to recognize b -hadrons for further processing. Moreover, the b -quark production cross section drops almost exponentially with the transverse momentum of the produced b quark. This puts the trigger threshold for b -physics events on a collision course with the experiment's data acquisition (DAQ) bandwidth.

All b physics triggers at CDF and $D\phi$ are based on leptons, with the possibility of requiring both single leptons and dileptons events. As an example, CDF dilepton trigger consists of a dimuon trigger with $P_T > 2$ GeV/ c for both muon legs, and an $e\mu$ trigger with $P_T^\mu > 3$ GeV/ c and $E_e^e > 5$ GeV. The dimuon trigger is the source of the J/ψ sample, and both dilepton triggers are used for b mixing analysis. The thresholds for single-lepton triggers are higher with $P_T > 7.5$ GeV/ c for muons and $E_T > 8$ GeV

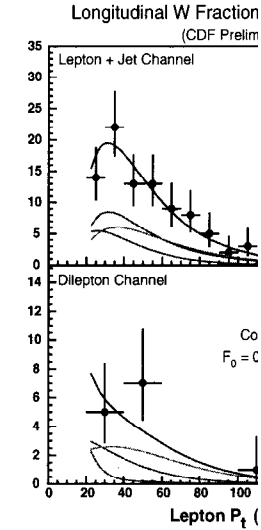


Figure 18: The CDF lepton P_T spectra for the sum of longitudinal W boson decays, transverse background.

for electrons. Analyses involving semileptonic decays are based on these single lepton triggers.

The publications from CDF and DØ on the field of b -physics have been numerous. In the last year alone (1998), many papers have documented the results from the two experiments on b -quark production,³⁷ lifetimes,³⁸ rare decays,^{39,40} and $B^0-\bar{B}^0$ mixing.⁴¹

In Sec. 4.1, we will concentrate on two recent results from CDF; the discovery of the B_c meson, and the first measurement at a hadronic collider of the time-dependent asymmetry in the decay $B^0, \bar{B}^0 \rightarrow J/\psi K_S^0$ with a low-statistics determination of the CP-violation parameter $\sin(2\beta)$.

4.1 Discovery of the B_c

During recent decades, quark spectroscopy has evolved in the same manner as atom and isotope spectroscopy did during the first half of this century. Just as the periodic table was built, one can build a quark periodic table also, as shown in Fig. 19(a).

One of the last missing items in the quark periodic table was the B_c , a very tight bound state of the two heaviest quarks (b and c) with a lifetime long enough to allow hadronization into a bound system. Nonrelativistic QCD potential models are expected to give a reliable description of an interesting spectroscopy with many states below the level for direct $B-D$ production, as shown in Fig. 19(b). The same models predict a B_c mass between 6.2 and 6.3 GeV/c^2 , and the lifetime is between 0.4 and 1.4 ps. Although significantly shorter than those of other B mesons, the B_c lifetime is expected to be measurable with the CDF SVX detector. Fragmentation models predict that the B_c production is suppressed by $\simeq 10^{-3}$ with respect to the production of B_d and B_u mesons.

Many exclusive B_c decay modes have been explored by the CDF and LEP experiments.⁴² Although a few candidates were found, their number was so low that no clear claim could be put forward. For this search, CDF⁴³ investigated the semileptonic decay with a J/ψ in the final state, as shown in Fig. 20(a). The J/ψ is reconstructed through the decay $J/\psi \rightarrow \mu^- \mu^+$ which is required at trigger level.

After the J/ψ candidate's reconstruction, shown in Fig. 20(a), the two muons and the third lepton are required to come from a common displaced secondary vertex. Due to the presence of the undetected ν in the final state, the only measurable quantities are the mass and the pseudolifetime of the tripleton system. The pseudolifetime ct^* is

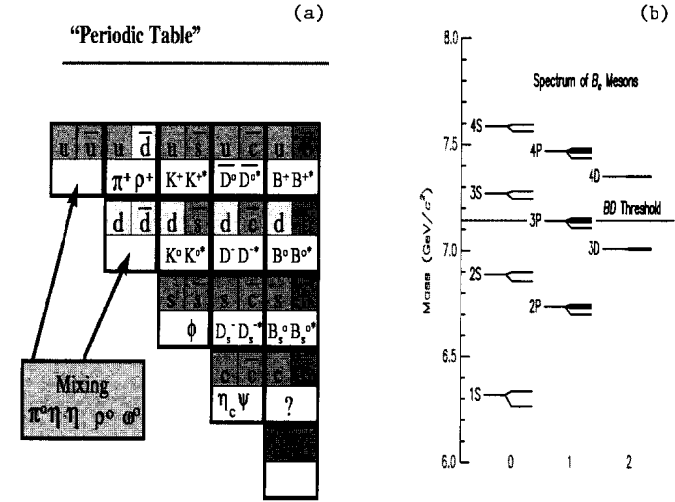


Figure 19: (a) Quark Periodic Table, and (b) level expectations for the bound states of b and c quarks.

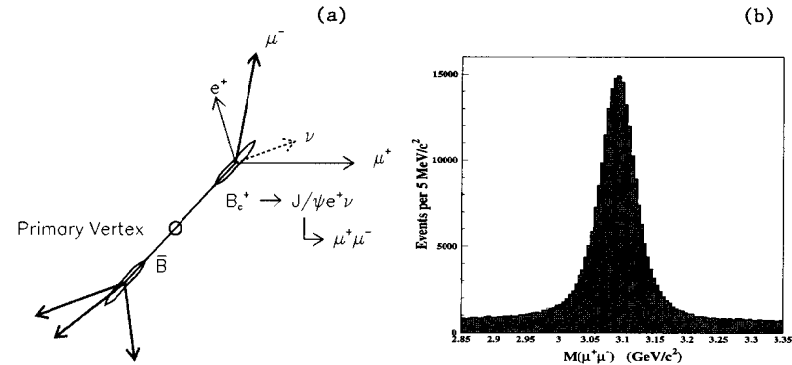


Figure 20: (a) Decay pattern for $B_c \rightarrow J/\psi l X$, and (b) invariant mass of $\mu^+ \mu^-$ pairs showing the J/ψ candidates.

defined as

$$ct^* = \frac{L_{xy} \times M(J/\psi l)}{P_T(J/\psi l)},$$

where L_{xy} is the distance between the reconstructed decay vertex and the average beam position in the transverse plane.

From Monte Carlo studies (where M_{B_c} is set to $6.27 \text{ GeV}/c^2$) most signal events are expected to have $4 \leq M(J/\psi l) \leq 6 \text{ GeV}/c^2$. To select possible decays of long lived particles, CDF requires $ct^* > 60 \mu\text{m}$. This cut is removed later for the lifetime measurement.

Starting with a sample of 196,000 J/ψ reconstructed in the SVX and then rejecting candidates compatible with being $B^+ \rightarrow J/\psi K^+$ decays, and events where the electron was identified as coming from a photon conversion, CDF finds a sample of 31 $J/\psi l$ candidates (19 $J/\psi e$, and 12 $J/\psi \mu$). The main sources of background are expected to be due to real J/ψ which form a good displaced vertex when paired with a hadron misidentified as a third lepton, and to $b\bar{b}$ events with one B hadron decaying to a J/ψ and the other B hadron decaying semileptonically, with a topology compatible with having the J/ψ and the lepton in a common vertex. Hadrons misidentified as the third lepton are found to be the main source of background. For muons, this is due to light hadrons (pions or kaons) which punch through the calorimeter and are then detected in the muon chambers, or decays in flight producing a muon with a kink small enough to be well-linked to the track of the hadron. For electrons, this happens when the shower of a hadron in the electromagnetic calorimeter is indistinguishable from that of an electron. The contribution of these sources is estimated from a $J/\psi + \text{track}$ sample obtained by releasing the lepton identification criteria on the third track. This sample is then weighted with the probability, estimated from real data as a function of P_T , that a hadron is misidentified as a lepton. With this method, CDF also obtains the mass shape of the background. Real $J/\psi l$ background from $b\bar{b}$ events is estimated from a Monte Carlo simulation.

A summary of all the background sources and the estimated signals in both channels is given in Table 6.

The number of B_c mesons and the statistical significance of the excess is also estimated from a likelihood fit of the $J/\psi l$ mass distribution, as shown in Fig. 21(a). The mass shapes for the signal and background are constrained to the results of signal simulation and background measurement, respectively. The only free parameter returned by the fit is the number of B_c mesons, $N(B_c) = 20.4^{+6.2}_{-5.5}$. The null hypothesis (i.e., the

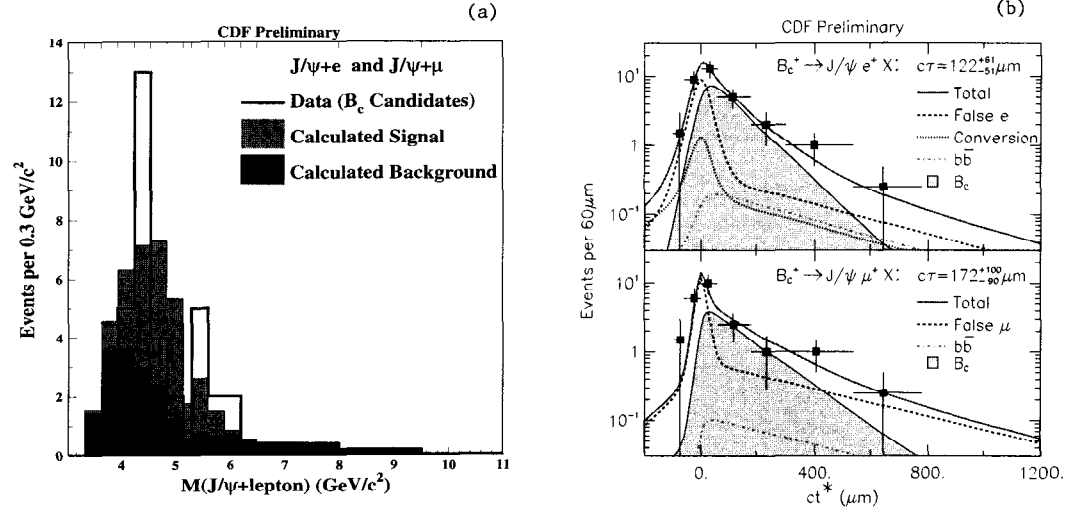


Figure 21: (a) Mass distribution of B_c candidates. The result of the fit for the B_c signal and the measured background are superimposed. (b) Pseudolifetime distribution for data (crosses) with the result of the fit for signal (shaded histogram) and background (dashed line).

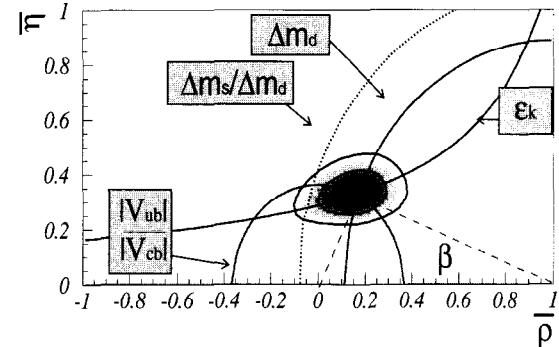


Figure 22: Indirect constraints⁴⁴ on the unitary triangle.

Table 6: Summary of the background sources and signal events estimates for a $J/\psi l$ mass between 4 and 6 GeV/c².

	$J/\psi e$ results	$J/\psi \mu$ results
False Electrons	$2.6 \pm 0.05 \pm 0.3$	
Conversions	$1.2 \pm 0.8 \pm 0.4$	
Total False Muons		$6.4 \pm 0.5 \pm 1.3$
Punch-Through		$0.88 \pm 0.13 \pm 0.33$
Decay-in-Flight		$5.5 \pm 0.5 \pm 1.3$
$B\bar{B}$ Background	1.2 ± 0.5	0.7 ± 0.3
Total Background	5.0 ± 1.1	7.1 ± 1.5
Events Observed	19	12
Net Signal	14.0	4.9
$P_{counting}(\text{Null})$	2.1×10^{-5}	0.084

probability for the background to generate the observed distribution) is rejected at the 4.8σ level.

To determine the B_c mass, the observed $J/\psi l$ mass distribution is fitted to different mass templates generated assuming a B_c mass between 5.5 and 7.5 GeV/c². CDF finds

$$M_{B_c} = 6.40 \pm 0.39(\text{stat.}) \pm 0.13(\text{syst.}) \text{ GeV}/c^2.$$

The B_c lifetime is determined by a fit to the pseudolifetime ct^* distribution shown in Fig. 21(b), where the background is parameterized by a prompt contribution plus negative and positive exponentials, while the signal is parameterized by a single positive exponential on which a statistical correction for the missing neutrino P_T is applied. Both background and signal distributions are convoluted with the experimental resolution on the decay length. The fit returns:

$$c\tau_{B_c} = 137_{-49}^{+53} \mu\text{m}.$$

From this, CDF infers a lifetime of $0.46 \pm 0.16 \pm 0.03$ ps, thus favoring the hypothesis that the c quark decays first and almost independently of the b quark.

The production rate for the B_c meson is determined by measuring the ratio

$$\frac{\sigma(B_c^+) \cdot Br(B_c^+ \rightarrow J/\psi l \nu)}{\sigma(B_u^+) \cdot Br(B_u^+ \rightarrow J/\psi K^+)} = 0.132_{-0.037}^{+0.041}(\text{stat.}) \pm 0.031(\text{syst.})_{-0.020}^{+0.032}(\text{lifet.}).$$

In this ratio, the uncertainties in the J/ψ trigger well as the luminosity determination, cancel. Six, the theoretical uncertainty on the b -quark production is larger. The CDF data are consistent with the theoretical prediction obtained by the LEP experiments.

4.2 Measurement of the CP Asymmetry

Since its discovery³ over thirty years ago in K^0 decays, CP violation has been a central topic in the matter-antimatter asymmetry of the universe and a priority of many high-energy physics programs. At the heart of CP violation lies in the relationship between the masses and mixing of different generations of quarks if three or more quark generations exist. In the Standard Model (SM), this relationship is parameterized by the unitary

$$\begin{pmatrix} d' \\ s' \\ b' \end{pmatrix} = \begin{pmatrix} V_{ud} & V_{us} & V_{ub} \\ V_{cd} & V_{cs} & V_{cb} \\ V_{td} & V_{ts} & V_{tb} \end{pmatrix} \begin{pmatrix} d \\ s \\ b \end{pmatrix}$$

where d , s , and b are the mass eigenstates and d' , s' , and b' are the weak eigenstates. With three generations, this matrix can be made capable of accommodating CP violation. As mentioned in the 1973 proposal of a third-quark generation to explain the unexpected discovery of the charmonium states with a fourth generation.

The CKM matrix is a unitary matrix, and one can express it as:

$$V_{ud}V_{ub}^* + V_{cd}V_{cb}^* + V_{td}V_{tb}^* = 0$$

This equation can be represented as a triangle in the complex plane.

By measuring enough quantities in the triangle, one can constrain and cross-check the basic parameters of the CKM matrix. The angle β , is shown in Fig. 22 and expressed as:

$$\beta \equiv \arg\left(-\frac{V_{cd}V_{cb}^*}{V_{td}V_{tb}^*}\right).$$

β can be measured by comparing the relative decay rates of B^0 and \bar{B}^0 to the common CP eigenstate mode $J/\psi K_S^0$. By exploiting the interference between the direct decay path ($B^0 \rightarrow J/\psi K_S^0$) and the mixed decay path ($B^0 \rightarrow \bar{B}^0 \rightarrow J/\psi K_S^0$), β can be measured through the time-dependent asymmetry

$$A_{CP} = \frac{\bar{B}^0(t) - B^0(t)}{\bar{B}^0(t) + B^0(t)} = \sin(2\beta) \sin(\Delta m_d t),$$

where $B^0(t)$ and $\bar{B}^0(t)$ are the number of decays to $J/\psi K_S^0$, at the time t , assuming that the meson produced at $t = 0$ was a B^0 or a \bar{B}^0 , respectively. The effect of the mixing between B^0 and \bar{B}^0 appears through the mass difference Δm_d , while the CP-phase difference between the two decay amplitudes appears via the factor $\sin(2\beta)$. Indirect evidence shown in Fig. 22 implies $0.30 < \sin(2\beta) < 0.88$ at 95% C.L., while OPAL recently reported⁴⁵ $\sin(2\beta) = 3.2_{-2.0}^{+1.8} \pm 0.5$ using the same decay channel.

During Run I, CDF collected approximately 200 $B^0, \bar{B}^0 \rightarrow J/\psi K_S^0$ decays. Although this sample is not sufficient to allow a precise measurement of $\sin(2\beta)$, it is the largest reconstructed sample of $B^0, \bar{B}^0 \rightarrow J/\psi K_S^0$ decays in the world, and it can be studied⁴⁶ to determine the feasibility of this measurement in a hadron collider. As for the B_c discovery, the selection of $B^0, \bar{B}^0 \rightarrow J/\psi K_S^0$ candidates starts from the $J/\psi \rightarrow \mu^+ \mu^-$ reconstruction. The muon tracks are required to be measured in the SVX detector, thereby obtaining a precise determination of the J/ψ vertex. The other pairs of oppositely charged tracks in the event are then searched for those consistent with the $K_S^0 \rightarrow \pi^+ \pi^-$ decay hypothesis, where the K_S^0 decay point is significantly displaced from the J/ψ vertex. Each K_S^0 candidate is then combined with the J/ψ candidate in a four-particle fit which requires the K_S^0 to point back to the J/ψ vertex, and the combined $J/\psi K_S^0$ system to point back at the primary vertex. The mass calculated by the fit has a typical resolution of $\sigma_M \sim 9 \text{ MeV}/c^2$. The proper decay length has a typical resolution of $\sim 50 \mu m$. Figure 23(a) shows the distribution of positive-lifetime candidate events as a function of the normalized mass $M_N = (M_{FIT} - M_0)/\sigma_{FIT}$, where M_0 is the central value of the B^0 mass peak ($5.277 \text{ GeV}/c^2$). A maximum likelihood fit yields 198 ± 17 mesons. Since the CP asymmetry varies in time as $\sin(\Delta m_d t)$, it reaches its maximum close to a proper decay length of $\sim 1000 \mu m$, which is a region in which the background is strongly suppressed, as shown in Fig. 23(b).

4.2.1 Same-Side Flavor Tagging

Once the sample of B 's is obtained, the next step is to determine ("tag") whether they were B^0 's or \bar{B}^0 when they were produced.

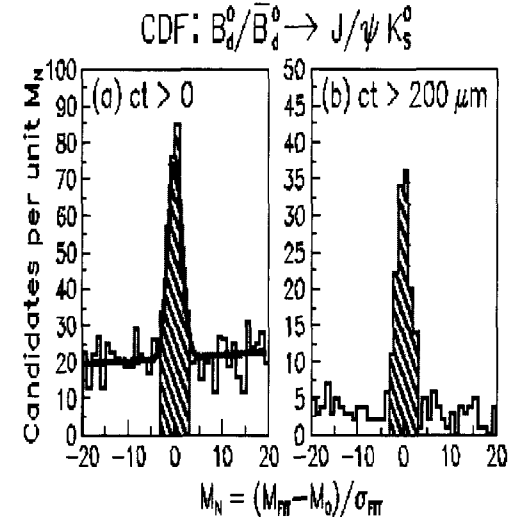


Figure 23: Normalized mass distribution for (a) $B^0 \rightarrow J/\psi K_S^0$ candidates with $ct \geq 0$, and (b) $ct \geq 200 \mu m$. The curve is the Gaussian signal plus background from the full likelihood fit.

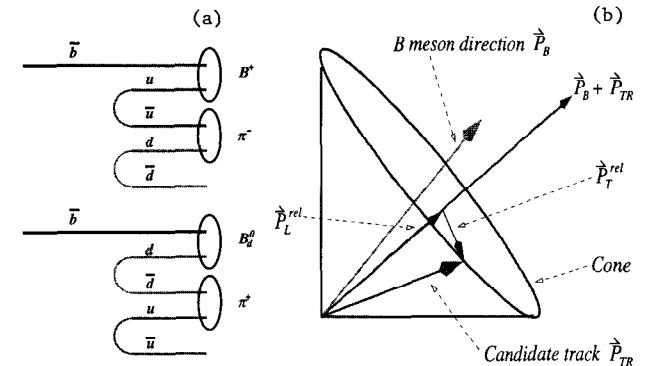


Figure 24: (a) A simple picture of b quarks hadronizing into B mesons, and (b) definition of tagging candidate based on P_T^{rel} .

Different methods have been suggested for this tagging. Most of them rely on the “opposite-side tagging,” i.e., the identification of the flavor of the second b in the events through its semileptonic decay ($b \rightarrow e^-$, while $\bar{b} \rightarrow e^+$), or its decay into charged Kaons. Similarly, the Opposite Side Jet-Charge method reconstructs the away-side b -hadron and uses statistical methods to determine its flavor. Alternatively, one can consider the “same-side tagging” (SST), i.e., the determination of the b quark flavor through the examination of the particles produced in association with the reconstructed B . In particular, the method used by CDF relies on the correlation between the flavor of the reconstructed B and the charge of a nearby particle. This idea was first proposed in order to take advantage of the fact that the b quark may first hadronize to a B^{**} state, whose decay products would be the B^0 as well as a “tagging” pion:⁴⁷

$$\begin{aligned} B^{*-} &\rightarrow \bar{B}^0 \pi^-, \\ B^{*+} &\rightarrow B^0 \pi^+. \end{aligned}$$

In this scenario, a \bar{B}^0 would always be associated with a π^- , and a B^0 with a π^+ . The same correlation is expected to exist between the B meson and the “leading” pion from fragmentation, as shown in Fig. 24(a), and the CDF analysis utilizes both sources of correlation. The nearby track is selected according to the following criteria:

- the track must lie in an $\eta - \phi$ cone with a half-angle of 0.7, around the B meson direction,
- $P_T^{min} \geq 400$ MeV/c, and
- the track must consistently be coming from the primary vertex.

When there is more than one candidate track, the one with the smallest P_T^{rel} is selected as the tagging track, as shown in Fig. 24(b). P_T^{rel} is defined as the component of the particle momentum transverse to the momentum of the combined $B + particle$ system.

The tagging algorithm, based upon physical processes that happen before the B meson decays, is applicable to other decay modes, and indeed, it has been applied successfully to the observation of the $B^0 - \bar{B}^0$ mixing and the measurement of Δm_d using the $B \rightarrow lD^{(*)}X$ decay,⁴⁸ as shown in Fig. 25.

The same algorithm has been applied for a measurement of the mixing parameter Δm_d in a lower-statistic sample of $B^0 \rightarrow J/\psi K^*$ decays (which kinematically are very similar to the $J/\psi K_S^0$ decays used for the CP measurement) yielding a measurement of Δm_d consistent with the higher precision determination of Fig. 25.

If the tagging algorithms were perfect, the time-dependent mixing measurement

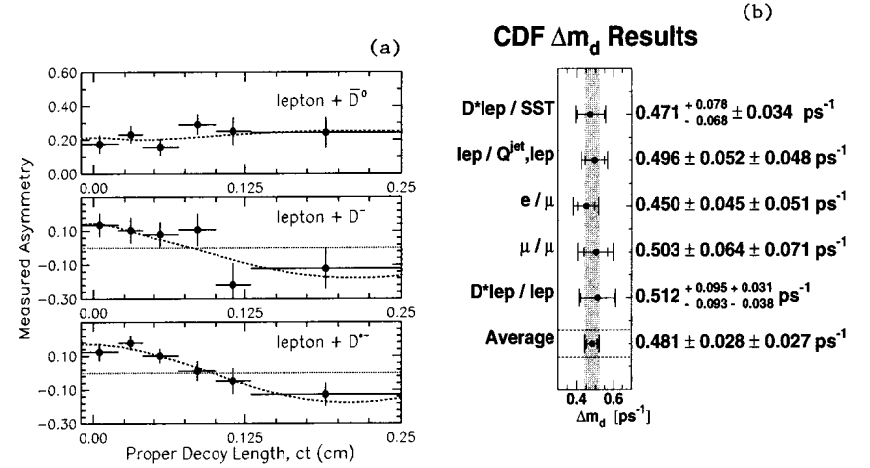


Figure 25: (a) Measured tagging asymmetries as a function of ct for $B \rightarrow l + D^0$ candidates (coming mostly from B^+), where no mixing is expected, and $B \rightarrow l + D^{(*)-}$ (coming mostly from B^0) for which mixing is expected. (b) Compilation of Δm_d measurements from CDF, showing that the SST method is competitive with the other standard methods.

shown in Fig. 25(a) would be a cosine curve of amplitude one. An amplitude smaller than one is an indication of a “dilution” of the measurement. The dilution, \mathcal{D}_0 , is related to the mistag probability and to the observed asymmetry by:

$$\begin{aligned} A_{CP}^{obs} &= \mathcal{D}_0 \sin(2\beta) \sin(\Delta m_d t), \\ \mathcal{D}_0 &\equiv \frac{N_{RS} - N_{WS}}{N_{RS} + N_{WS}} = 1 - 2\mathcal{P}_{mistag}, \end{aligned}$$

where N_{RS} are events with the correct-sign correlation, and N_{WS} events with the wrong-sign correlation. For this same-side tagging method, $\mathcal{D}_0 \sim 20\%$. This dilution determination, measured on the data, is necessary for the extraction of $\sin(2\beta)$.

4.2.2 Tagging Asymmetry

The SST technique tags approximately 65% of the $B^0, \bar{B}^0 \rightarrow J/\psi K_S^0$ decays. Figure 26 shows the sideband-subtracted asymmetry in bins of the proper decay-time, where the asymmetry is calculated by counting the sideband-subtracted number of positive tags, N^+ , and negative tags, N^- , in each proper decay-time bin:

$$\mathcal{A}(ct) = \frac{N^-(ct) - N^+(ct)}{N^-(ct) + N^+(ct)}.$$

The signal and background samples were defined according to the dashed region shown in Fig. 23. The events in the signal region generally prefer negative tags (i.e., a positive asymmetry), whereas events in the sideband regions favor positive tags (negative asymmetry). As noted before, however, the signal purity is high at large ct , and the sideband subtraction is, correspondingly, a small effect.

Two fits are shown in Fig. 26. The dashed curve gives the results of a simple χ^2 fit of the function $\mathcal{A}_0 \sin(\Delta m_d t)$ to the binned asymmetries, where Δm_d has been fixed to its 1996 world-averaged⁴⁹ value of 0.474 ps^{-1} . The solid curve is the result of an unbinned maximum likelihood fit which incorporates both signal and background distributions in mass and proper decay-time. Sideband and negative-lifetime events are included to help constrain the background distributions. The likelihood function also incorporates resolution effects and corrections for systematic biases, such as the small inherent charge asymmetry favoring positive tracks resulting from the wire plane orientation in the main CDF drift chamber. Clearly, the result is dominated by the sample size and not by the particular fitting procedure applied to the data. Also shown

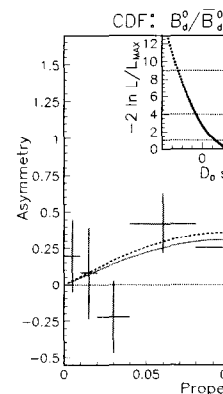


Figure 26: The sideband-subtracted tagging asymmetry versus proper decay length (point discussed in the text, while the inset shows t

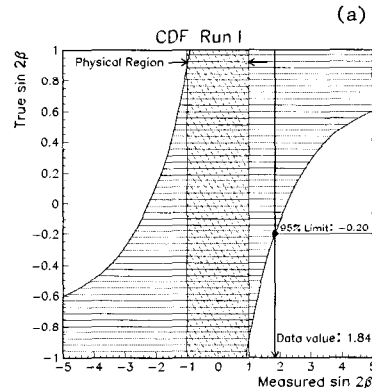


Figure 27: 95% confidence belts for the sin(2β) measurement; (a) intersection with the actual measurement interval, and (b) the world summary of sin(2β)

in the Fig. 26 inset is the relative log-likelihood. It is very close to a parabola, indicating Gaussian errors.

Before entirely ascribing the above asymmetry to CP Violation, all other sources of charge asymmetry must be eliminated. The small charge asymmetry of the main drift chamber has been measured in an independent sample of inclusive $B \rightarrow J/\psi X$ decays and corrected for in the maximum likelihood fit. Backgrounds from other B decays, such as $B^0 \rightarrow J/\psi K^{*0}$, $K^{*0} \rightarrow K_S^0 \pi^0$, and $B^0 \rightarrow J/\psi K^+$, where the π^0 has not been reconstructed, have been considered and found to be negligible. The high signal purity at large decay times also limits contributions to the asymmetry from backgrounds which are present in the sidebands. CDF determines the systematic uncertainty on $\mathcal{D}_0 \sin(2\beta)$ by shifting the central value of each fixed input parameter of the likelihood fit by $\pm 1\sigma$ and refitting it to find the shift in $\mathcal{D}_0 \sin(2\beta)$.

The following systematic effects were investigated:

- B^0 lifetime,
- parametrization of the intrinsic charge asymmetry of the detector, and
- Δm_d .

The systematic effects are added in quadrature, giving

$$\mathcal{D}_0 \sin(2\beta) = 0.31 \pm 0.18(\text{stat.}) \pm 0.03(\text{syst.}).$$

4.2.3 Extracting $\sin(2\beta)$

As mentioned above, the dilution \mathcal{D}_0 , which reduces the amplitude of the CP asymmetry, can be measured in other data samples, including the $B^0 \rightarrow J/\psi K^{*0}$ decays and the $B^0 \rightarrow lD^{(*)}X$ samples. These different dilution measurements can be extrapolated to the kinematic range appropriate for the $J/\psi K_S^0$ data. The extrapolation is done using a Monte Carlo simulation based upon a version of the PYTHIA event generator tuned to CDF data;⁴⁶ the necessary adjustments to the different dilutions are at the level of 10% at most, and CDF finds that the appropriate dilution for the $B^0 \bar{B}^0 \rightarrow J/\psi K_S^0$ data is $\mathcal{D}_0 = 0.166 \pm 0.018 \pm 0.013$, where the first uncertainty is due to the uncertainties in the contributing dilution measurements, and the second uncertainty is due to the Monte Carlo extrapolation, which is calculated by varying the parameters of the Monte Carlo model. Using this value of \mathcal{D}_0 , CDF finds

$$\sin(2\beta) = 1.8 \pm 1.1(\text{stat.}) \pm 0.3(\text{syst.}),$$

where the dilution uncertainty has been added to the systematic uncertainty. The central value is unphysical since the amplitude of the measured asymmetry exceeds the measured dilution. The result may be phrased in terms of confidence intervals. The CDF analysis follows the frequentist construction of Feldman and Cousins,⁵⁰ which gives proper confidence intervals even for measurements in the unphysical region, as is the case here. The confidence interval is shown in Fig. 27(a). It is found that the measurement corresponds to an exclusion of $\sin(2\beta)$ values below -0.20 at 95% C.L.

It is also interesting to note that as long as $\mathcal{D}_0 \neq 0$, then the exclusion of negative $\sin(2\beta)$ from this result is independent of the actual value of \mathcal{D}_0 . Given that $\mathcal{D}_0 > 0$, the same prescription for calculating a limit yields an exclusion of negative values of $\sin(2\beta)$ at 90% C.L. Figure 27(b) shows the world summary of the direct measurements of $\sin(2\beta)$. Clearly, one of the priorities for future experiments is to bring $\sin(2\beta)$ into the physical region!

5 Prospects for Run II

After the termination of Run I in February 1996, the accelerator and both detectors at Fermilab started a program of major upgrades for the next data taking period (Run II), which is expected to start in the year 2000. The major addition to the accelerator complex is the Main Injector, a 150 GeV machine that will be used to inject protons into the Tevatron and will replace the Main Ring in the creation of antiprotons. The Main Injector is expected to increase the Tevatron peak luminosity from $\sim 2 \times 10^{31} \text{ cm}^{-2} \text{ s}^{-1}$ to $\sim 8 \times 10^{31} \text{ cm}^{-2} \text{ s}^{-1}$. A second machine, the Recycler, will capture unused antiprotons at the end of a collider run and reuse them, boosting the peak luminosity to $\sim 2 \times 10^{32} \text{ cm}^{-2} \text{ s}^{-1}$. In addition, the Tevatron energy will increase from $\sqrt{s} = 1.8 \text{ TeV}$ to $\sqrt{s} = 2 \text{ TeV}$, thus boosting the $t\bar{t}$ cross section by 40%. The total integrated luminosity expected to be delivered to the experiments during Run II is $\sim 2 \text{ fb}^{-1}$. Both collider detectors are being upgraded⁵¹ for Run II. The major upgrades include: DØ acquiring a tracking system with a central solenoidal magnetic field and a silicon vertex detector, and CDF expanding the coverage of its vertex detector, its calorimetry, and its muon detectors.

5.1 Potentials for Top Physics in Run II

The reach of top physics at the Tevatron during Run II has been studied.⁵² Each detector will record ~ 160 dilepton and ~ 1200 lepton+jets events, with ~ 500 of them double-tagged. For the cross-section measurement, the limiting factor will probably be the error on the luminosity, which can be measured to $\sim 5\%$ using the $W \rightarrow l\nu$ rate. Therefore, the error on the production cross section is expected to be around 8–10%.

The error on the mass measurement is presently dominated by statistics, but the uncertainty on the jet energy scale is a close second. As it is usual in the study of systematic errors, the understanding of the energy scale will likely improve with improving statistics (by studying, for instance, the $Z + multijet$ events). The total uncertainty on M_{top} in Run II should be at the level of $2 \text{ GeV}/c^2$ (i.e., at the 1% level).

The precision on the R measurement should improve to 2%, corresponding to a 95% C.L. of $|V_{tb}| \geq 0.20$, while limits of $B(t \rightarrow q\gamma) < 3 \times 10^{-3}$ and $B(t \rightarrow qZ) < 0.02$ should be achievable.

From single top production, which is directly proportional to $|V_{tb}|^2$, the Tevatron experiments will be able to determine $|V_{tb}|^2$ to $\sim 10\%$. Other fields of study may arise from the large top quark mass and the *expected* (or, rather, *hoped for*) connection with the symmetry breaking mechanism of the Standard Model.

5.2 Potentials for B Physics in Run II

The goal of the B physics community in the next decade is the measurement of the unitary triangle parameters. Therefore, we will concentrate on the expectations for this kind of physics, even though it is expected that the Tevatron experiments will continue exploring the “standard” b physics avenues, like lifetimes, B^0 and B_s mixing, and heavy states searches.

Studies of CP violation will concentrate on the measurement of $\sin(2\beta)$ and $\sin(2\alpha)$ in $B^0 \rightarrow J/\psi K_s^0$ and $B^0 \rightarrow \pi^+\pi^-$ decays. CDF has demonstrated that the Tevatron Collider environment allows these kind of measurements. Moreover, CDF plans to also look for CP violation in $B_s \rightarrow D_s K$ and $B \rightarrow DK$, probing $\sin(2\gamma)$.

As shown in the discussion of the $\sin(2\beta)$ measurements, the important ingredients for the CP measurements are the efficiency ϵ to tag the original b flavor and the dilution \mathcal{D} in the tagging. These ingredients are combined in a figure of merit ($\epsilon\mathcal{D}^2$) that compares different tagging methods, since the error on the determination of a given CP asymmetry is proportional to $1/\sqrt{N\epsilon\mathcal{D}^2}$, where N is the number of reconstructed

decays. The $\epsilon\mathcal{D}^2$ for the three tagging methods discussed in the CP asymmetry measurements at CDF are shown in Table 7.

Table 7: Summary of the *dilepton* counting experiments.

Tagger	$\epsilon\mathcal{D}^2$ (Run I)	$\epsilon\mathcal{D}^2$ (Run II)	Relevant Upgrade
Soft Lepton (SLT)	0.9 ± 0.1	1.7	Extended Coverage
Same Side π (SST)	1.7 ± 0.2	2.0	New Tracking
Jet Charge (JetQ)	1.0 ± 0.4	3.0	New Tracking
All Combined	2.9	5.4	

Based on the experience gathered in Run I, CDF expects to reconstruct $\sim 10,000$ $B^0 \rightarrow J/\psi K_s^0$ decays in Run II. This takes into account the increased luminosity, the extended silicon vertex detector, and the upgraded muon detector. This expectation is conservative because it does not include the possibility of using the $J/\psi \rightarrow e^+e^-$ decay channel, which will be possible in Run II with a contribution of ~ 5000 more reconstructed B^0 decays. The asymmetry and its error are defined as:

$$\begin{aligned} \mathcal{A} &= \mathcal{D} \sin 2\beta, \\ \sigma(\sin 2\beta) &= \frac{\sigma(\mathcal{A})}{\mathcal{D}} \oplus (\sin 2\beta) \frac{\sigma(\mathcal{D})}{\mathcal{D}}, \end{aligned}$$

where \oplus means addition in quadrature. Using the values determined in the Run I analysis and extrapolating according to Table 7, CDF expects to measure $\sin(2\beta)$ with an error of $\sigma(\sin 2\beta) = 0.071 \oplus 0.044 = 0.08$.

The identification and reconstruction of $B \rightarrow \pi^+\pi^-$, for the determination of $\sin(2\alpha)$, is very challenging at hadronic colliders because of the very low branching ratio ($\sim 10^{-5}$) and the huge combinatorial background from the low P_T charged tracks produced in $p\bar{p}$ collisions. CDF made an effort to study the trigger and the background rejection. A fully dedicated trigger, based on the idea of selecting tracks with large impact parameter ($d_0 \geq 100\mu\text{m}$) is thought to be sufficient to limit the event rate. Assuming 10,000 events in 2 fb^{-1} , $\epsilon\mathcal{D}^2 = 5.4\%$ and a signal-to-background ratio of one to four, CDF expects to measure the asymmetry with an error of $\sigma_{\mathcal{A}} = 0.12$.

References

- [1] M. Perl *et al.*, Phys. Rev. Lett. **35**, 1489 (1975).
- [2] N. Cabibbo, Phys. Rev. Lett. **10**, 531 (1963).
M. Kobayashi and T. Maskawa, Prog. Theor. Phys. **49**, 652 (1973).
- [3] J. Christenson *et al.*, Phys. Rev. Lett. **13**, 138 (1964).
- [4] S. W. Herb *et al.*, Phys. Rev. Lett. **39**, 252 (1977).
- [5] C. Berger *et al.*, (PLUTO), Phys. Lett. B **76**, 243 (1978); C. W. Darden *et al.*, (DASP), Phys. Lett. B **76**, 246 (1978).
- [6] C. Itzykson, J.-B. Zuber, *Quantum Field Theory* (McGraw-Hill, New York 1980).
- [7] W. Behrens *et al.*, (JADE), Phys. Lett. B **146**, 437 (1984).
- [8] The LEP Collaborations ALEPH, DELPHI, L3 OPAL, the LEP Electroweak Working Group, and the SLD Heavy Flavor Group:
D. Abbaneo *et al.*, LEPEWWG/97-02.
- [9] V. Bharadwa *et al.*, 10th Topical Workshop on $p\bar{p}$ Collider Physics, Fermilab, May 1995.
- [10] F. Abe *et al.*, Nucl. Instr. Methods A **271**, 387 (1988).
- [11] P. Azzi *et al.*, Nucl. Instr. Methods A **360**, 137 (1995); FERMILAB-CONF-94/205-E;
D. Amidei *et al.*, Nucl. Instr. Methods A **350**, 73 (1994).
- [12] S. Abachi *et al.*, Nucl. Instr. Methods A **338**, 185 (1994).
- [13] C. Albajar *et al.*, Phys. Lett. B **186**, 247 (1987).
- [14] H. Albrecht *et al.*, Phys. Lett. **192**, 245 (1987).
- [15] C. Quigg, presented at the *Advanced School on Electroweak Theory*, Mao, Menorca, 1996, FERMILAB-CONF-97/157-T, hep-ph/9707508.
- [16] F. Abe *et al.*, Phys. Rev. D **50**, 2966 (1994);
F. Abe *et al.*, Phys. Rev. Lett. **73**, 225 (1994).
- [17] F. Abe *et al.*, Phys. Rev. Lett. **74**, 2626 (1995).
- [18] S. Abachi *et al.*, Phys. Rev. Lett. **74**, 2632 (1995).
- [19] J. Rosner, "Top Quark Mass," presented at the *NATO Advanced Study Institute on Masses of Fundamental Particles*, Cargese, France, 1996. CERN-TH-96-245, hep-ph/9610222.
- [20] E. Laenen *et al.*, Phys. Rev. Lett. B **321**, 2 (1998).
- [21] E. Berger and H. Contopanagos, Phys. Rev. Lett. **74**, 2632 (1995).
- [22] S. Catani *et al.*, Phys. Lett. B **378**, 329 (1996).
- [23] F. Abe *et al.*, Phys. Rev. Lett. **80**, 2779 (1998).
- [24] S. Abachi *et al.*, Phys. Rev. Lett. **79**, 1203997 (1997).
- [25] F. Abe *et al.*, Phys. Rev. Lett. **80**, 2773 (1998).
- [26] F. Abe *et al.*, Phys. Rev. Lett. **79**, 1992 (1997).
- [27] B. Abbott *et al.*, FERMILAB-PUB-98/133 (1998), hep-ph/9801133, to Phys. Rev. D.
- [28] B. Klima, presented at the *12th Les Renccontres de Physique de la Vallée d'Aoste: Results and Perspectives in Particle Physics*, La Thuile, 1998, FERMILAB-CONF-98/137-E, hep-ex/980117.
- [29] F. Abe *et al.*, Phys. Rev. Lett. **80**, 2767 (1998);
F. Abe *et al.*, Phys. Rev. Lett. **82**, 271 (1999), hep-ph/9801133.
- [30] S. Abachi *et al.*, Phys. Rev. Lett. **79**, 1197997 (1997).
- [31] B. Abbott *et al.*, Phys. Rev. Lett. **80**, 2063998 (1998).
- [32] G. Quast, *29th International Conference on High Energy Physics*, Vancouver, BC, CANADA; see also <http://www.cern.ch/HEP98>.
- [33] F. Abe *et al.*, in *Proceedings of International Conference on High Energy Physics (HEP 97)*, Jerusalem, Israel 1997.
- [34] S. Glashow *et al.*, Phys. Rev. D **2**, 1285 (1970).
- [35] F. Abe *et al.*, in *Proceedings of 33rd Rencontres de Physique de la Vallée d'Aoste: High Energy Hadronic Interactions*, Les Arcs, France, 1997, hep-ph/9707508, E.
- [36] B. Abbott *et al.*, Phys. Rev. Lett. **74**, 2548995 (1995);
B. Abbott *et al.*, Phys. Lett. B **370**, 239 (1996).
- [37] B. Abbott *et al.*, Phys. Rev. Lett. **82**, 35 (1999).
- [38] F. Abe *et al.*, Phys. Rev. D **57**, 5382 (1998).
- [39] F. Abe *et al.*, Phys. Rev. D **57**, R3811 (1998).
- [40] B. Abbott *et al.*, Phys. Lett. B **423**, (1998).

- [41] F. Abe *et al.*, Phys. Rev. Lett. **80**, 2057 (1998).
- [42] P. Abreu *et al.*, Phys. Lett. B **398**, 207 (1997);
K. Ackerstaff *et al.*, Phys. Lett. B **420**, 157 (1998);
R. Barate *et al.*, Phys. Lett. B **402**, 213 (1997).
- [43] F. Abe *et al.*, Phys. Rev. Lett. **81**, 2432 (1998).
- [44] F. Parodi *et al.*, LAL-98-49, hep-ph/9802289 (1998).
- [45] K. Ackerstaff *et al.*, Eur. Phys. J. C **5**, 379 (1998).
- [46] F. Abe *et al.*, Phys. Rev. D **59**, 32001 (1999).
- [47] M. Gronau, A. Nippe, and J. L. Rosner, Phys. Rev. D **47**, 1988 (1993);
M. Gronau and J. L. Rosner, Phys. Rev. D **49**, 254 (1994).
- [48] F. Abe *et al.*, Phys. Rev. Lett. **80**, 2057 (1998);
F. Abe *et al.*, Phys. Rev. D **59** 32001 (1999).
- [49] Particle Data Group; R. Barnett *et al.*, Phys. Rev. D **54**, 1 (1996).
- [50] G. Feldman and R. Cousins, Phys. Rev. D **57**, 3873 (1998).
- [51] CDF Collaboration, FERMILAB-PUB-96/390-E, 1996;
D ϕ Collaboration, FERMILAB-PUB-96/357-E, 1996.
- [52] The TeV-2000 Group Report, FERMILAB-PUB-96/082, 1996; R. Frey *et al.*,
FERMILAB-CONF-97/085 1997.